Investigating Hector Convective Development and Microphysical Structure Using High-Resolution Model Simulations, Ground-Based Radar Data, and TRMM Satellite Data

SABRINA GENTILE AND ROSSELLA FERRETTI

Department of Physical and Chemical Sciences/CETEMPS, University of L'Aquila, L'Aquila, Italy

FRANK SILVIO MARZANO

Department of Information Engineering/CETEMPS, Sapienza University of Rome, Rome, Italy

(Manuscript received 3 April 2013, in final form 22 November 2013)

ABSTRACT

One event of a tropical thunderstorm typically observed in northern Australia, known as Hector, is investigated using high-resolution model output from the fifth-generation Pennsylvania State University–National Center for Atmospheric Research (PSU–NCAR) Mesoscale Model (MM5) observations from a ground-based weather radar located in Berrimah (Australia) and data from the Tropical Rainfall Measuring Mission (TRMM) satellite. The analysis is carried out by tracking the full life cycle of Hector from prestorm stage to the decaying stage. In both the prestorm stage, characterized by nonprecipitating cells, and the triggering stage, when the Hector storm is effectively initiated, an analysis is performed with the aid of high-spatial-and-temporal-resolution MM5 output and the Berrimah ground-based radar imagery. During the mature ("old") stage of Hector, considering the conceptual model for tropical convection suggested by R. Houze, TRMM Microwave Imager satellite-based data were added to ground-based radar data to analyze the storm vertical structure (dynamics, thermodynamics, and hydrometeor contents). Model evaluation with respect to observations (radar reflectivity and TRMM data) suggests that MM5 performed fairly well in reproducing the dynamics of Hector, providing support to the assertion that the strength of convection, in terms of vertical velocity, largely contributes to the vertical distribution of hydrometeors. Moreover, the stages of the storm and its vertical structure display good agreement with Houze's aforementioned conceptual model. Finally, it was found that the most important triggering mechanisms for this Hector event are topography, the sea breeze, and a gust front produced by previous convection.

1. Introduction

The tropical thunderstorm Hector is one of the tallest convective cells on Earth (it may reach 20 km in depth) and represents one of the main processes for the exchange between upper-tropospheric and lower-stratospheric air. Zipser et al. (2006) studied the intensity of storms using proxies for convective strength; these parameters are based on the Tropical Rainfall Measuring Mission (TRMM) satellite data. In this study the event shows a minimum brightness temperature at 85 GHz detected by the TRMM Microwave Imager (TMI) lower than 50 K (not shown). Therefore, based on the Zipser et al. (2006) classification, it belongs to the most extreme [0.001% in Fig. 2 in Zipser et al. (2006)] fraction of the total events collected in their paper.

Hector develops almost diurnally over the Tiwi Islands (consisting of Melville and Bathurst islands, located near Darwin in the northern tropical part of Australia) during the transition and break season, with maximum activity in the early afternoon. Hector is a storm developing over a relatively flat region, and despite being one of the most studied long-lived thunderstorms, its vertical structure is not yet completely understood and the low predictability of such a system makes its forecasting practice a still challenging problem (Keenan and Carbone 1992; Carbone et al. 2000; Ferretti and Gentile 2009).

Several campaigns were held in Australia with the aim of improving the understanding of this thunderstorm:

Corresponding author address: Sabrina Gentile, Department of Physical and Chemical Sciences/CETEMPS, University of L'Aquila, Via Vetoio, 67010 Coppito - L'Aquila, Italy.
E-mail: sabrina.gentile@aquila.infn.it

DOI: 10.1175/JAS-D-13-0107.1

Island Thunderstorm Experiment during 1988 (ITEX), Maritime Continent Thunderstorm Experiment during 1995 (MCTEX), Stratospheric–Climate Links with Emphasis on the Upper Troposphere and Lower Stratosphere during late 2005 (SCOUT-O3), and Tropical Warm Pool–International Cloud Experiment during early 2006 (TWP-ICE). All of them helped to characterize Hector and to improve the modeling of the storm itself. Based on measurements collected during the MCTEX campaign, Carbone et al. (2000) classified Hector events depending on the forcing mechanisms leading to the storm initiation and development. If the convective cell is triggered by the collision of the sea-breeze fronts from the northern and southern coasts of the islands, the storm is classified as type A; type B results from the collision of one of the sea-breeze fronts and a gust front generated by earlier convection. Additional studies based on idealized numerical experiments and case studies also contributed to the understanding of the forcing and the triggering mechanisms of this convective cell (e.g., Golding 1993; Crook 2001; Saito et al. 2001; Ferretti and Gentile 2009). Golding (1993) performed a study for two Hector events using the Met Office (UKMO) mesoscale model at 3-km horizontal grid spacing initialized with a local sounding. In this study, a strong relationship between storm development and island topography was found. He also concluded that a model resolution of at least 4 km is necessary for correctly simulating Hector.

Crook (2001) performed a study using both linear and nonlinear models for determining the most important parameters controlling the dynamics of Hector convective system. Low-level moisture was found to be an important parameter for differentiating between types A and B. Moreover, his study found a strong link between the total condensate (sum of all hydrometeors) of Hector cells and convective available potential energy (CAPE), wind speed, and direction.

One Hector event detected during the MCTEX campaign was investigated by Saito et al. (2001) using the Meteorological Research Institute nonhydrostatic model (MRI-NHM) at 1-km horizontal grid spacing. The study analyzed the life cycle of the storm assessing the development of Rayleigh–Bénard convection inland ahead of the sea-breeze front (Saito et al. 2001) in the early stage of Hector. Moreover, using results from sensitivity tests assessing the role played by the ice phase on the storm dynamics, the authors highlighted a strong link between the intensity of the updraft and the ice phase itself.

To further investigate the influence of the sea breeze and parameters such as water vapor content, land use, and soil moisture content in the triggering of the Hector storm, Ferretti and Gentile (2009) performed several numerical experiments for two real Hector events that developed during the SCOUT-O3 and TWP-ICE campaigns. Their results showed that an increase in soil moisture content inhibited the storm initiation because of the evaporational cooling; they also analyzed the role of the sea breeze in Hector development performing a numerical experiment where the onset of the sea-breeze front was prevented.

The observation-based conceptual model proposed by Houze (1989, 1997) describes the life cycle of a tropical convective system, which includes the transition from the vigorous convection stage to the stratiform stage. Since Hector is a clear example of a strong convective system in the tropics, it is reasonable to expect that Houze's model would be applicable to describe its evolution.

In this study, the high-resolution numerical simulations together with TRMM data will be used to investigate the compatibility of Houze's conceptual model with the Hector dynamics. In addition, seeking a more detailed understanding of the storm development, a combined analysis at high temporal resolution of the vertical velocity and hydrometeor fields is conducted. This is a necessary approach because among the physical mechanisms influencing the growth of the Hector storm that have not been exhaustively analyzed are the microphysical processes. In this context, observations describing the horizontal and vertical distribution of the hydrometeors in the storm are very useful, such as the satellite platforms that provide information about the three-dimensional fields of hydrometeors by using microwave radar and radiometer. The TRMM mission—a joint space mission between the National Aeronautics and Space Administration (NASA) and the Japan Aerospace Exploration Agency (JAXA)—is among these platforms, being designed to monitor and study tropical rainfall (Kummerow et al. 2000).

In this framework, the goal of this study is to investigate the dynamics and microphysics of a Hector event using TMI data, ground-based radar reflectivity, and high-resolution model simulations. The new contribution from this study is an observation-based (satellite- and ground-based radar) and model-aided analysis at high-space–time resolution of Hector development at the following stages:

- the preconvective phase, consisting of thermal plumes developing over warm surface until precipitation starts;
- the triggering phase, when the sea-breeze front advances farther inland and triggers convection because of both orographic lifting and convergence with gust fronts generated by previous convective activity; and
- the mature or ''old'' stage, for evaluating the compatibility of Houze's conceptual model in describing Hector's evolution.

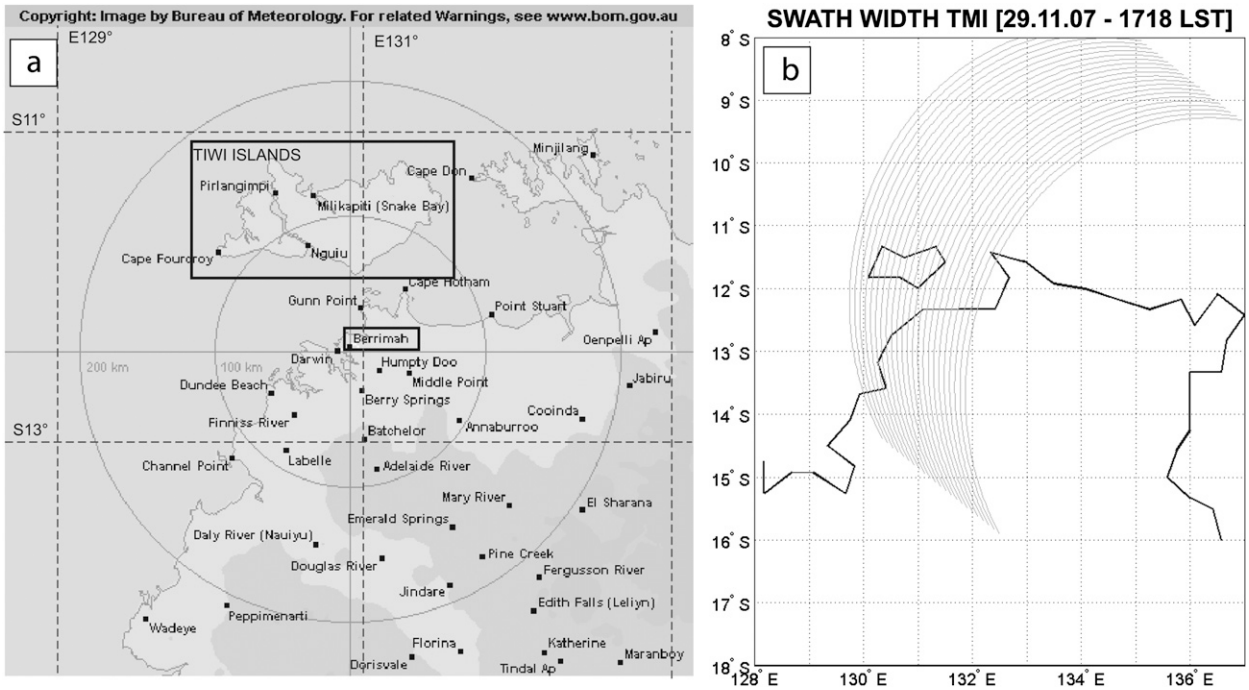

FIG. 1. (a) Berrimah radar location with good coverage in the Tiwi Islands' direction (source: http://www.bom.gov.au). (b) TRMM Microwave Imager satellite swath width at the surface at 1718 LST 29 Nov 2007.

Model simulations are employed to examine the preconvective, triggering, and mature phases of Hector; ground radar data are used to study the triggering and mature stages, while TMI data are used only for the mature stage.

The study is organized as follows. The main characteristics of the observational platforms measurements (Berrimah radar) as well as TRMM's mission goals and products are described in section 2. A brief meteorological overview of the Hector event is presented in the section 3; in section 4, the model configuration is presented. In section 5 the results are discussed, focusing on the Hector phases using model simulation, observed radar reflectivity, and TRMM hydrometeor profiles. Finally, section 6 summarizes the results and gives some concluding remarks.

2. Description of the remote sensing data

a. The Berrimah radar

The Berrimah radar is a C-Band single-polarization radar located approximately 7 km southeast of Darwin Airport (12.46°S, 130.93°E); it is intermittently used for research purposes, so it may be unavailable for some extended periods (Radar Site Information–Australian Government Bureau of Meteorology website: http://www.bom.gov.au/australia/radar/info/nt_info.shtml#berrimah63). Berrimah radar has a good coverage in all directions up to a range of 250 km, allowing for observing the reflectivity over the Tiwi Islands (Fig. 1a), but heavy rain over the radar site will cause attenuation of the signals. Path attenuation also occurs when the radar beam crosses an intense thunderstorm cell; the returned signal from cells will be reduced so rain echoes may appear less intense than actual rainfall rate, if not properly corrected using dual-polarization capability if present (e.g., Vulpiani et al. 2005).

b. TRMM satellite mission

TRMM is the first mission dedicated to the observation of the tropical rainfall and its feedback on global climate (Kummerow et al. 2000), and it is a joint mission of NASA and JAXA. TRMM's primary instruments for measuring precipitation are the Precipitation Radar (PR), TMI, and the Visible and Infrared Scanner (VIRS). In this study, only TMI is used owing to its relatively wide swath; it is a passive microwave sensor designed to provide quantitative rainfall information over a 760-km-wide swath (Fig. 1b). By collecting brightness temperatures at five microwave frequencies—namely, 10.7, 19.4, 21.3, 37.0, and 85.5 GHz—TMI is able to retrieve the integrated water vapor, cloud water gross profile, and rainfall intensity. An important characteristic of TMI product is its high resolution at the ground level (5 km) owing to the low altitude of TRMM (approximately 402 km).

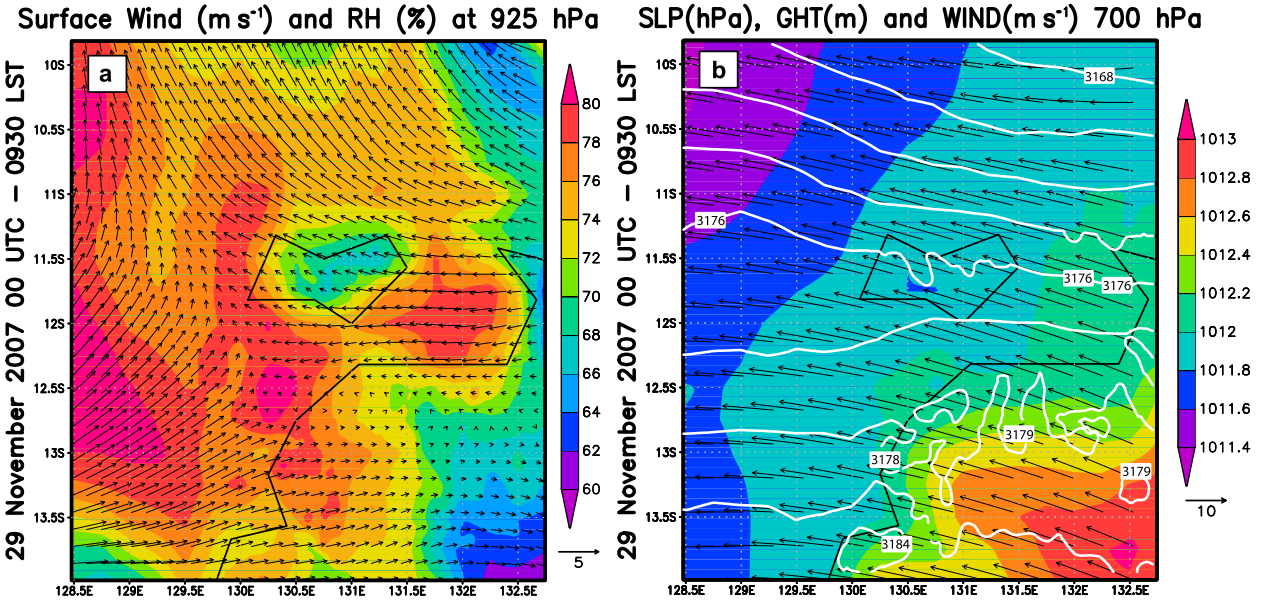

FIG. 2. ECMWF analysis at 0930 LST 29 Nov 2007: (a) surface wind (m s^{-1}) and relative humidity at 925 hPa (filled color; %); (b) sea level pressure (filled color; hPa), geopotential height at 700 hPa (white contours; m), and horizontal wind vectors (m s^{-1}) at 700 hPa.

The data used in this work are acquired as part of the NASA's Earth–Sun System Division and archived and distributed by the Goddard Earth Sciences (GES) Data and Information Services Center (DISC). All TRMM science data products can be downloaded from a distributed Active Archive System at NASA's website; these data files, which are provided in the National Center for Supercomputing Applications (NCSA)'s Hierarchical Data Format (HDF), are generally distributed online (http://trmm.gsfc.nasa.gov/index.html). The TRMM data products used for this study are the 2A12 (Goddard Space Flight Center Distributed Active Archive Center 2007).

3. Meteorological characteristics of the Hector event

The Hector event selected for this study is chosen mainly on the basis of TMI data availability: 29 November 2007. The main meteorological characteristics of the Hector event are briefly presented using European Centre for Medium-Range Weather Forecasts (ECMWF) analysis and the available observations described in the previous section.

This event is characterized by a weak eastward flow (less than 5 m s^{-1}) at lower levels, advecting humid air toward Tiwi Islands (Fig. 2a), which is initially dryer than the surroundings. In addition, the meteorological conditions show the lack of low-level vertical shear and a moderate (10–12 m s^{-1}) horizontal wind at 700 hPa (Figs. 2a,b) as the soundings at 0000 UTC (0930 LST) and 1200 UTC (2130 LST) (Figs. 3a,b) show. Both soundings clearly show a layer of dry air before Hector development (0000 UTC) at upper levels (6000–7000 m; Fig. 3a), descending in the following hours down between 3000 and 5000 m (Fig. 3b). The weak low-level wind may favor the development of deep convective cells, as will be further discussed in the section 5a.

The 29 November 2007 Hector event develops during the transition season as confirmed by the easterly flow at 700 hPa (Fig. 2b); in fact, according to Keenan and Carbone (1992), break–transition season systems exist in a regime dominated by easterly wind at 3-km height. The geostationary satellite (visible channel; VIS) and radar imagery (Figs. 4 and 5) help in understanding Hector triggering mechanisms and evolution: the clouds would imply the two sea-breeze fronts (Fig. 4a) at 1203 LST; these are clearly nonprecipitating cells because no echoes are detected at this time from Berrimah radar. At 1503 LST, 3 h later, nonprecipitating convection is still implied by both the satellite (Fig. 4b), which shows clouds mostly along the east–west axis of the Tiwi Islands, and the radar imagery, which is not detecting any echoes yet. This would suggest an early stage of nonprecipitating convective cells typically developing because of cooler and wetter air blowing over a warm surface. By 1530 LST, precipitation starts in the western part of Melville Island, as the radar echoes confirm (Fig. 5a). At 1603 LST, the satellite image (Fig. 4c) shows clouds aligned along the major axis of the Tiwi Islands whose triggering

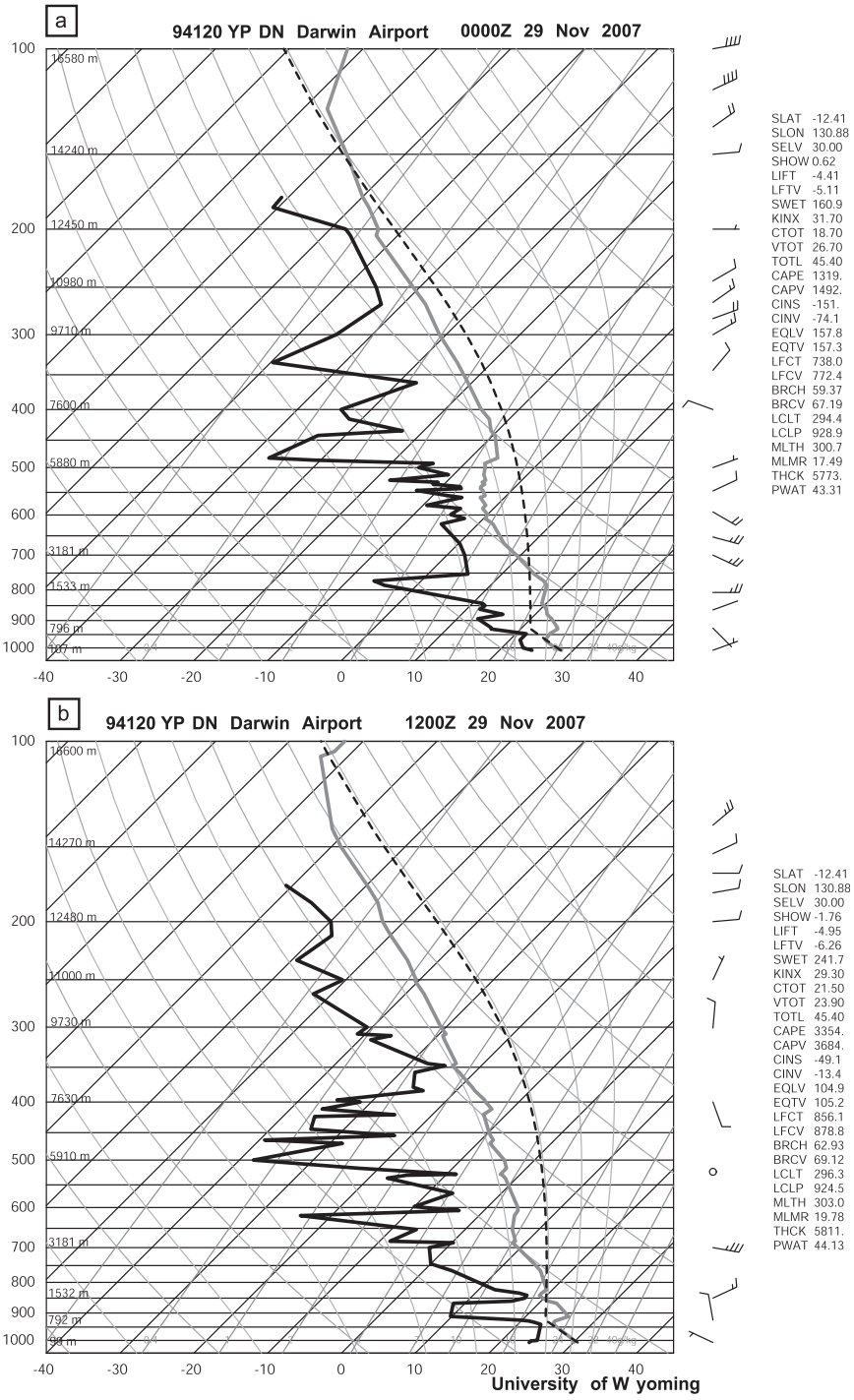

FIG. 3. Soundings at (a) 0000 UTC (0930 LST) and (b) 1200 UTC (2130 LST) 29 Nov 2007. Black line is dewpoint temperature; gray line is temperature.

mechanism may be the convergence of the two sea-breeze fronts; these are precipitating cells, as the radar echoes confirm (Fig. 5b). The cells quickly aggregate to form a precipitating convergence line at 1635 LST, extending east–west of the Tiwi Islands (Fig. 5c). In the following hour (1715 LST), rainfall reaches a maximum reflectivity of 60 dBZ (Fig. 5d) and the cell reaches the maximum vertical development, as the anvil would suggest (Fig. 4d). Later, the cell moves westward (Fig. 5e) and decays by 1930 LST (Fig. 5f). This rough analysis

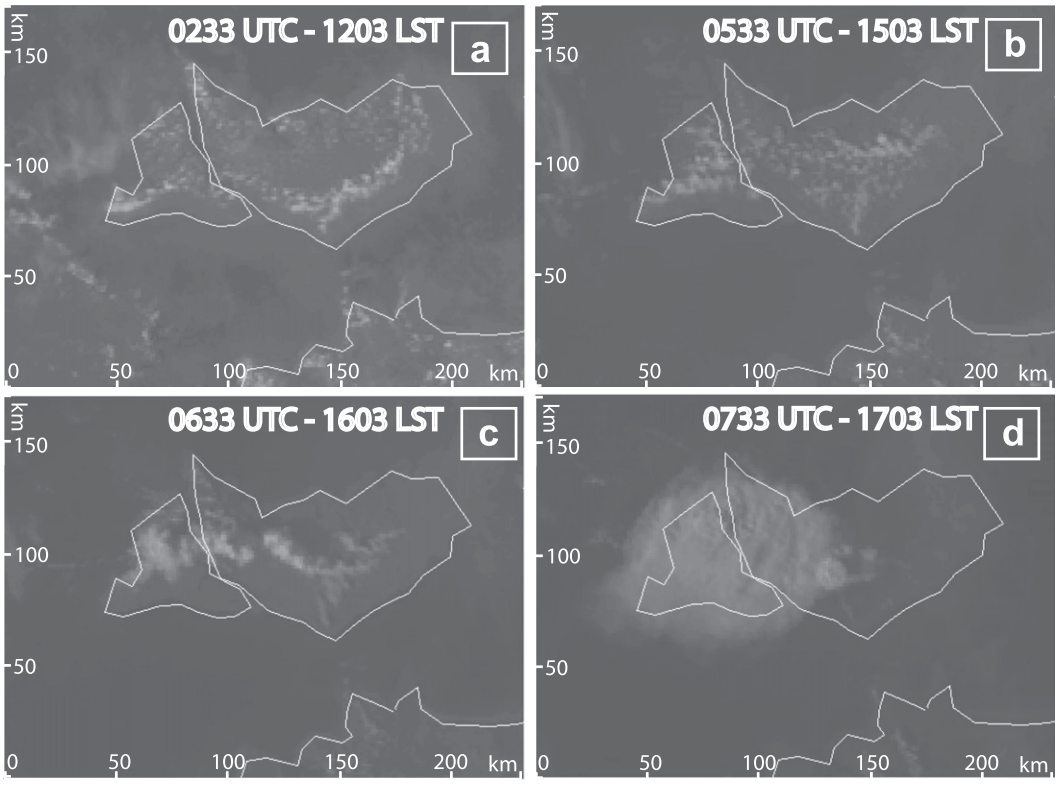

FIG. 4. *Geostationary Meteorological Satellite*-5 (*GMS*-5) visible images over the Tiwi Islands from (a) 1203 until (d) 1703 LST 29 Nov 2007. White area indicates cloud cover.

would suggest the convergence of the two sea-breeze fronts as the mechanism for generating the updraft for triggering Hector; therefore, this event should be classified as type A, following Carbone et al. (2000).

TMI captures the mature stage of the Hector cell as the anvil cloud suggests (Fig. 4d); this is also confirmed by the Berrimah radar detecting the maximum reflectivity (Fig. 5d) at the TRMM overpass on the Tiwi Islands at 1718 LST. The high value of the heating rate at high altitude (Fig. 6) supports the hypothesis of a mature stage at 1718 LST. The TMI observations show a Hector cell of approximately 20-km width and 18-km height (Fig. 6); the heating rate vertical structure supports the hypothesis of double mode: the lower-level maximum is probably the leftover of previous ''vigorous convection'' as defined by Houze (1997) in the conceptual model, whereas the upper-level one may be associated with ''old convection'' (Houze 1997)—that is, the stratiform part of the storm.

4. Model configuration

To better understand the triggering mechanism and the dynamical and microphysical evolution of Hector, high-resolution simulations are performed using the fifth-generation Pennsylvania State University–National Center for Atmospheric Research (PSU–NCAR) Mesoscale Model, version 3 (MM5V3). This is a nonhydrostatic model at primitive equations fully compressible with a terrain-following vertical coordinate (Dudhia 1993; Grell et al. 1994). The model has multiple nesting capabilities to improve the simulation over the area of interest. To this purpose, four nested domains are used: The mother domain has a 27-km grid, covering the tropical part of Australia. The finest domain has a horizontal grid of 1 km and it is centered over the Tiwi Islands (Fig. 7). Based on the preliminary tuning performed by Ferretti and Gentile (2009) to achieve the best configuration, the following is assumed:

- We use 58 unevenly spaced vertical levels from the surface to 20 hPa (approximately 26 km) with highest density in the boundary layer; the lowest level is at approximately 5 m [list of levels in Ferretti and Gentile (2009)].
- The Gayno–Seaman (GS) parameterization is used for the planetary boundary layer (PBL); this scheme is particularly feasible for humid area as the tropical one (Ballard et al. 1991; Shafran et al. 2000). The horizontal and vertical eddy diffusivity K are computed

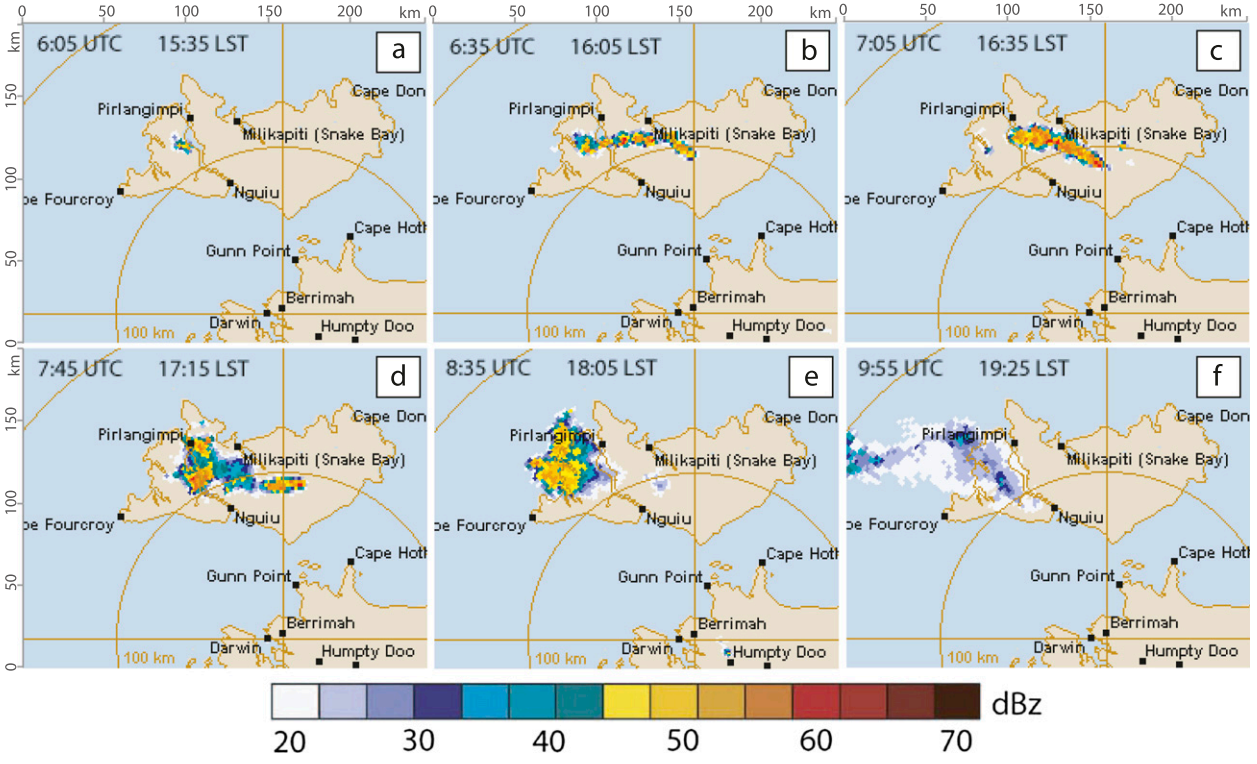

FIG. 5. Radar reflectivity (dBZ) from 1535 LST (0605 UTC) to 1925 LST (0955 UTC) 29 Nov 2007 observed from Berrimah radar (source: http://www.bom.gov.au).

differently: K_h is given by the horizontal deformation and a background value proportional to the grid size and the time step. The surface fluxes are provided by the surface layer and the land surface schemes. This scheme is characterized by a 2.5-order local approach (based on the Mellor–Yamada scheme) on PBL diurnal variations. The GS uses liquid water potential temperature Θ_l and total water mixing ratio q_t; the turbulent flux of Θ_l is parameterized using a counter gradient heat flux term that allows for representing also larger eddies (Stull 1988). Moreover, this scheme advects the turbulent kinetic energy (TKE).

- The MM5 cloud radiation scheme is used for radiative transfer processes (Dudhia et al. 2005).
- The Kain–Fritsch cumulus convection parameterization is applied to domains 1, 2, and 3, whereas no cumulus convective parameterization is used for the finest domain. This scheme exploits a sophisticated cloud-mixing scheme to compute the mass exchange between cloud and environment (entrainment–detrainment) as a function of the buoyancy characteristics of mixtures of clear and cloudy air (Kain and Fritsch 1993; Kain 2004).
- The Reisner 2 parameterization is used to evaluate the impact of microphysics on the simulation of the thunderstorm for all the domains. This parameterization is based on mixed-phase scheme but adding graupel and ice number concentration prediction equations (Reisner et al. 1998).

To the aim of investigating the role of the orography in the Hector triggering an extra simulation (named NOTOPO) is performed setting to zero the orography

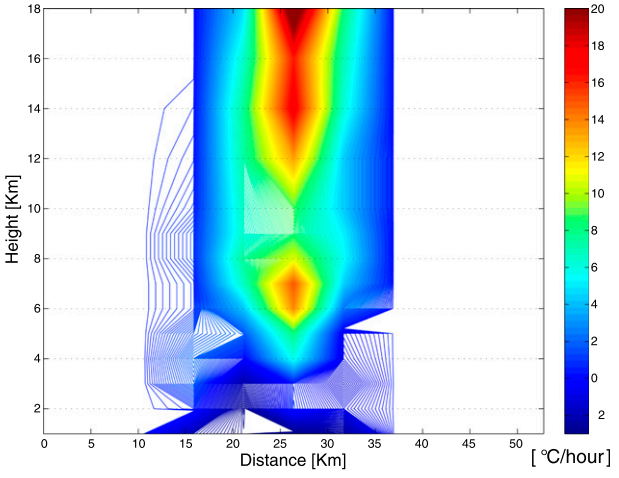

FIG. 6. Heating rate (°C h^{-1}) vertical cross section observed by TMI along the convective cell on 29 Nov 2007.

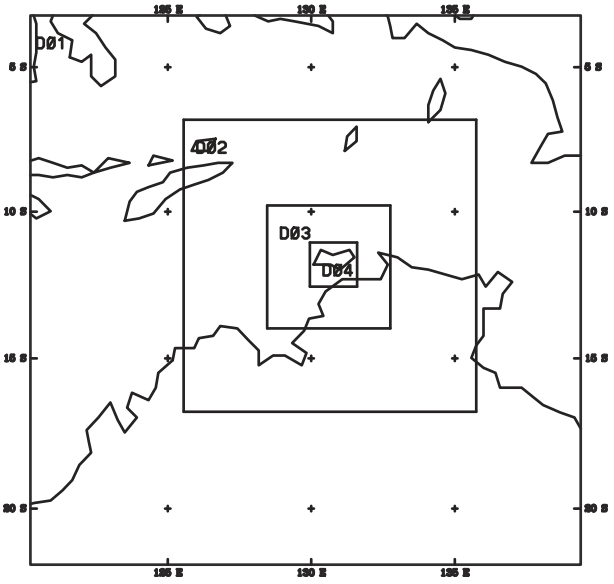

FIG. 7. The model domains. The horizontal resolution is 27 km for domain 1, 9 km for domain 2, 9 km for domain 3, and 1 km for domain 4. Domain 4 is centered on the Tiwi Islands.

of the southern side of the Tiwi Islands and using the same configuration as before. No impact is expected on the initial stage of Hector development because the first organized plumes develop in the northeastern side of the Tiwi Islands, where a convective unstable PBL set up. The impact of orography using the NOTOPO simulation will be analyzed during the following phases (triggering and mature).

The simulations are performed using the ECMWF 0.25° analysis as boundary and initial conditions; they last 24 h from 2130 LST (1200 UTC) 28 November to 2130 LST (1200 UTC) 29 November 2007.

5. Results

To the aim of outlining a conceptual model for the formation of Hector, high-resolution simulation and observation-aided study is performed in terms of surface (radar reflectivity and horizontal wind) and three-dimensional fields (vertical velocity and vertical profiles of hydrometeor) at different stages:

- in the early stage when nonprecipitating cells develop because the air is slowly blowing over a warm surface,
- during the triggering and the growth phase of Hector because of the interaction of the downdraft with either sea-breeze front or convergence forced by the topography, and
- at the mature stage in terms of microphysics using both MM5 results and TMI observation.

In the following analysis the model radar reflectivity is calculated using the default equation available in the MM5 postprocessing (Stoelinga 2009). This simulates an equivalent radar reflectivity factor, based on the mixing ratios of rain, snow, and graupel (if available). The equations that relate mixing ratios of rain, snow, and graupel to reflectivity factor are derived assuming spherical particles of constant density with exponential size distributions. The simulated radar reflectivity has been extracted at the level closer to the Berrimah radar one (approximately 30 m).

a. Pre-Hector phase: From the thermal plumes to the starting of the rain

The satellite imagery (Fig. 4a) at 1203 LST shows aligned clouds in the southeastern side of the Tiwi Islands; no echoes are recorded by the radar at this time, as their lack in Fig. 5 demonstrates. Three hours later, nonprecipitating (no echoes are detected by radar) convective clouds are still developing in the northeastern flank of the Tiwi Islands as the satellite imagery shows (Fig. 4b).

The MM5 output at high temporal and spatial resolution is used to investigate the origin of these convective cells and their time evolution. In what follows, the horizontal wind together with the MM5 radar reflectivity and the vertical cloud structure will be used to analyze the cell evolution located on the center of the Tiwi Islands. To ease the readability of the figure, only the central part of the Tiwi Islands will be shown (dashed area in Fig. 8). To analyze the vertical structure of the convective cells, both in the pre-Hector and maximum phase, two cross sections are taken: a fixed one is taken in the area where Hector will finally develop (the red line on the following figures) and the second one (the gray line in the following figures) will be moved together with the cells, starting from where the aligned nonprecipitating cells first appear.

By 1110 LST (0140 UTC), organized plume develops in the northeastern side of the Tiwi Islands, where a convective unstable PBL set up (not shown). Indeed, a vertical decreasing equivalent potential temperature θ_e in the first 3000 m of the atmosphere is present. In the following 20 min the thermal plume strengthened, injecting higher values of θ_e into the layer of lower values at the upper levels. The MM5 simulation produces (not shown) a layer of low θ_e between 2000 and 5000 m associated with preexisting dry air that acts as a blanket, producing a convective unstable PBL. In this environment, the plumes generated by the warm surface can turn in convective clouds and eventually precipitate. The maximum development associated with these aligned organized cells with a strong vertical temperature

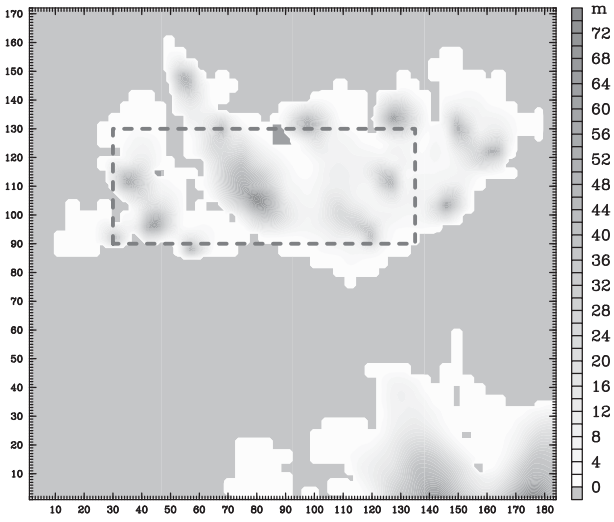

FIG. 8. Area of zoom.

gradient is found by 1210 LST. The cross section taken (gray line in Fig. 9c) through the organized thermal plumes in the northeastern side of Tiwi Island (Fig. 9a) (i.e., where the topography is not changed) clearly shows condensation starting at the upper levels, but precipitation has not started yet. The northern sea-breeze front entering inland warms up and starts to buoy; the warming process is enhanced by the low horizontal wind speed, which allows for the air slowly passing over the warm surface to have more time to warm up by sensible heat transfer. The plumes build up until condensation processes produce rainfall whose downdraft, interacting with the well-organized upward and downward motion, destroys these regular convective cells. The updrafts are stronger (approximately $200\,\mathrm{cm\,s^{-1}}$) than the downdraft (approximately $-80\,\mathrm{cm\,s^{-1}}$), as the simulated vertical velocity suggests (Fig. 9b, updraft shown as red lines and downdraft shown as blue lines), because of the associated latent heat released by the condensation of water vapor that increases the buoyancy. In addition, in the southwestern flank of the Tiwi Islands, high value of CAPE (Fig. 9c) can be clearly associated to the onset of the southern sea-breeze front. CAPE reaches values greater than $6000\,\mathrm{J\,kg^{-1}}$, confirming the advection of wet and warm air from the southwest. In the northern part, where the organized convective plumes appear (gray line in Fig. 9c), CAPE assumes relatively lower values (approximately $3000\,\mathrm{J\,kg^{-1}}$) owing to the downdraft that pumps dry and cold air from higher levels. By 1230 LST, condensation starts to produce precipitating cells in the western side of the aligned cells (Fig. 10a), ending the nonprecipitating convection phase. At this time, both sea-breeze fronts have not yet reached the center of the Tiwi Islands and no deep convection has developed yet (Fig. 9c, red line).

The previous analysis would suggest an MM5 temporal bias of approximately 2 h.

b. *From the organized plumes to the Hector triggering*

The comparison between MM5 and both Berrimah radar reflectivity and TMI data confirms a 2-h model time shift: MM5 produces cells fairly close to the one observed by Berrimah radar but 2 h in advance, and the Hector maximum development is reached 2 h in advance with respect to the maximum established from TMI. Therefore, in the following analysis, the comparison is performed accounting for a 2-h lag for the MM5 output to "get rid" of this time shift.

During the previous phase, both MM5 (Fig. 9c) and Berrimah radar (Fig. 5a) show few echoes only in the western side of the Tiwi Islands. A few cells start to condensate and produce rainfall (at 1230 LST, Figs. 10a,b); the associated gust front destroys the upward and downward motion of the organized convection. At this time, both sea-breeze fronts start moving inland, producing convection and a small precipitating cell that continuously develops and dissipates. By 1330 LST, the two sea-breeze fronts reach the Tiwi Islands' center; hence, a few cells start to develop because of the interaction between the southern sea-breeze front and gust fronts of decaying convective cells. Both MM5 at 1330 LST (Fig. 14a) and Berrimah radar at 1605 LST (Fig. 5b) clearly show echoes in the center of Tiwi Islands. The convergence of the sea-breeze front with the downdraft of decaying cells ensure a stronger upward motion, allowing the cells to grow above the PBL and to persist to the horizontal wind speed, which is much stronger above the PBL as the sounding shows (Fig. 3a). At 1350 LST, except for a 2-h bias, MM5 produces aligned precipitating convective cells (Fig. 14b) in good agreement with the ones observed by the satellite and radar (respectively, Figs. 4c and 5b). From this time, the strength of the southern sea breeze continues to increase, enhanced by the topography: the two hills in the southwestern side force the wind to blow in the small valley, reinforcing its strength and producing a convergence line, as is found in the southwestern part of the Tiwi Islands by 1410 LST (red arrow shown in Fig. 11b). The convection is already triggered as the strong simulated echoes suggest (Fig. 11a). The strong updraft produced by the convergence line interacts with the convective cells downdraft, generating the Hector embryo at MM5 time 1410 LST (Fig. 12a). Moreover, the latent heat released by the condensation processes warms up the convective tower, generating a discontinuity ("front") between the plume and the preexisting cold and dry air at upper layers (Fig. 12a). Hence, the descending tongue of cold and dry air lifts the Hector embryo, strengthening the upward motion (Fig. 12b).

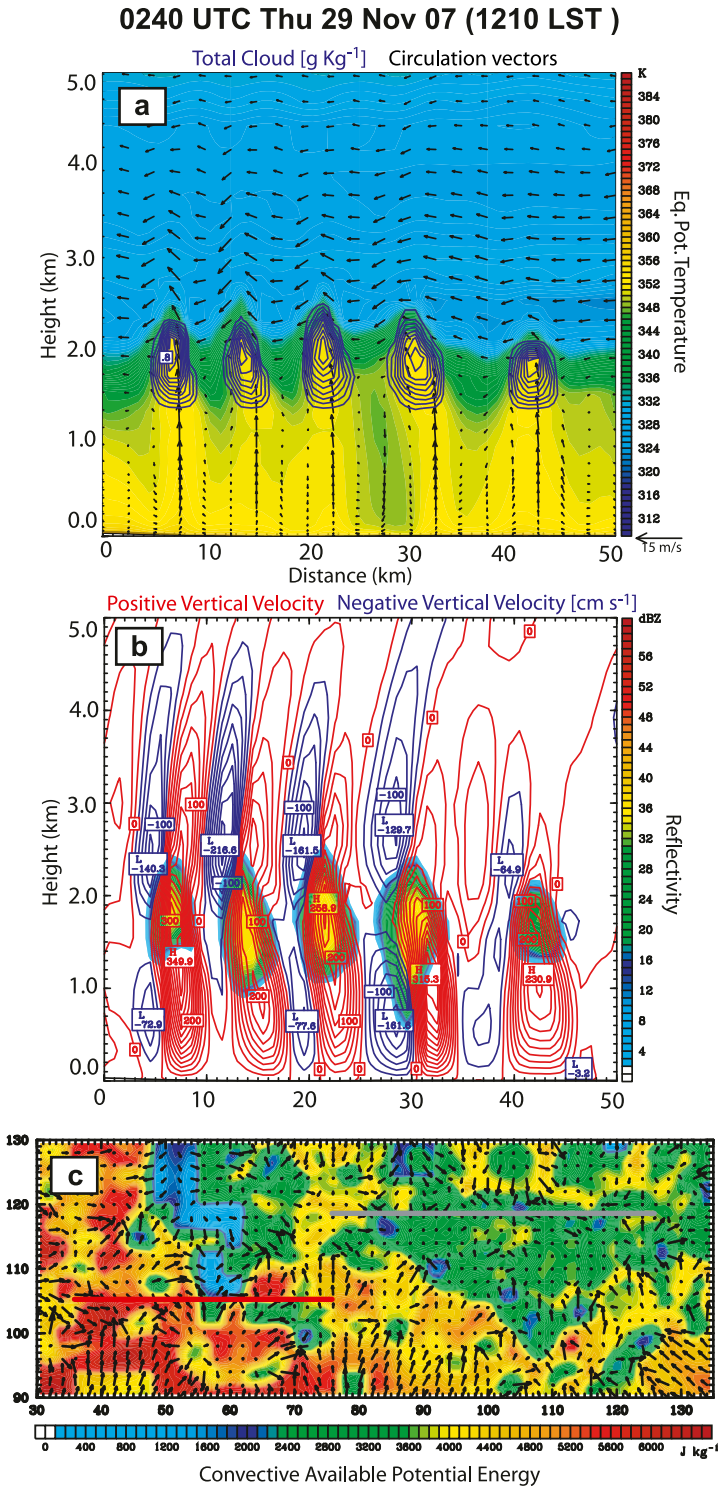

FIG. 9. Vertical sections of the simulated nonprecipitating cells; the section is taken along the solid gray line (red line indicates a fixed cross section not used now). (a) Total cloud mixing ratio (g kg^{-1}; blue contours), equivalent potential temperature (K; filled colors), and circulation vectors (arrows). (b) Positive and negative vertical velocity (cm s^{-1}; red and blue lines, respectively) and simulated radar reflectivity (dBZ; filled colors). (c) CAPE (J kg^{-1}; filled colors) and circulation vectors (arrows).

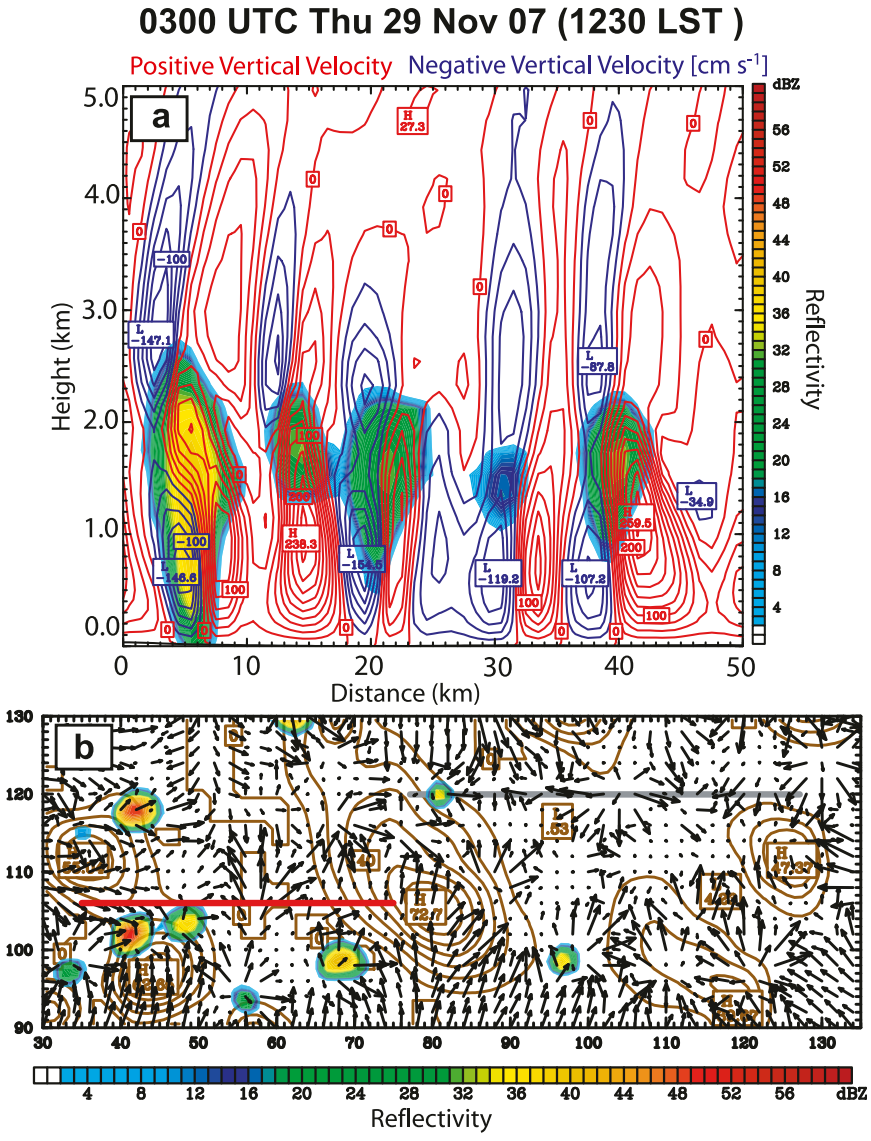

FIG. 10. Sections of the simulated precipitating cells; the vertical one is taken along the solid gray line (red line indicates a fixed cross section not used now). (a) Vertical simulated radar reflectivity (dBZ; filled color), positive and negative vertical velocity (cm s^{-1}; red and blue contours, respectively). (b) Horizontal simulated radar reflectivity (dBZ, filled color), topography (brown contour lines), and horizontal wind at the surface (arrows).

These are the basic ingredients for triggering Hector in the next 20 min. The previous hypothesis of the latent heat released by the condensation process enhancing the Hector raising motion is supported by the TMI-retrieved latent heat release at 1718 LST (Fig. 6), where large values are found at lower levels.

The role of topography in triggering Hector has been assessed by performing a simulation setting to zero the topography (NOTOPO) in the southern side of the Tiwi Islands. The southern sea breeze entering inland produces precipitating cells in the NOTOPO simulation (not shown) but the convergence line is not found and a much weaker Hector develops. Indeed, a shallower and thinner cell than the one produced by the control simulation is found in NOTOPO with a Hector reaching a maximum height of only 12–13 km. These strongly support the previous hypothesis of topography as one of the parameters for triggering Hector but not affecting the initial stage of the convective development.

In summary, the previous analysis performed using the MM5 high-spatiotemporal-resolution simulation and the radar reflectivity allows us to assess the triggering mechanisms for Hector except for a MM5 temporal bias. The analysis suggests the following Hector triggering

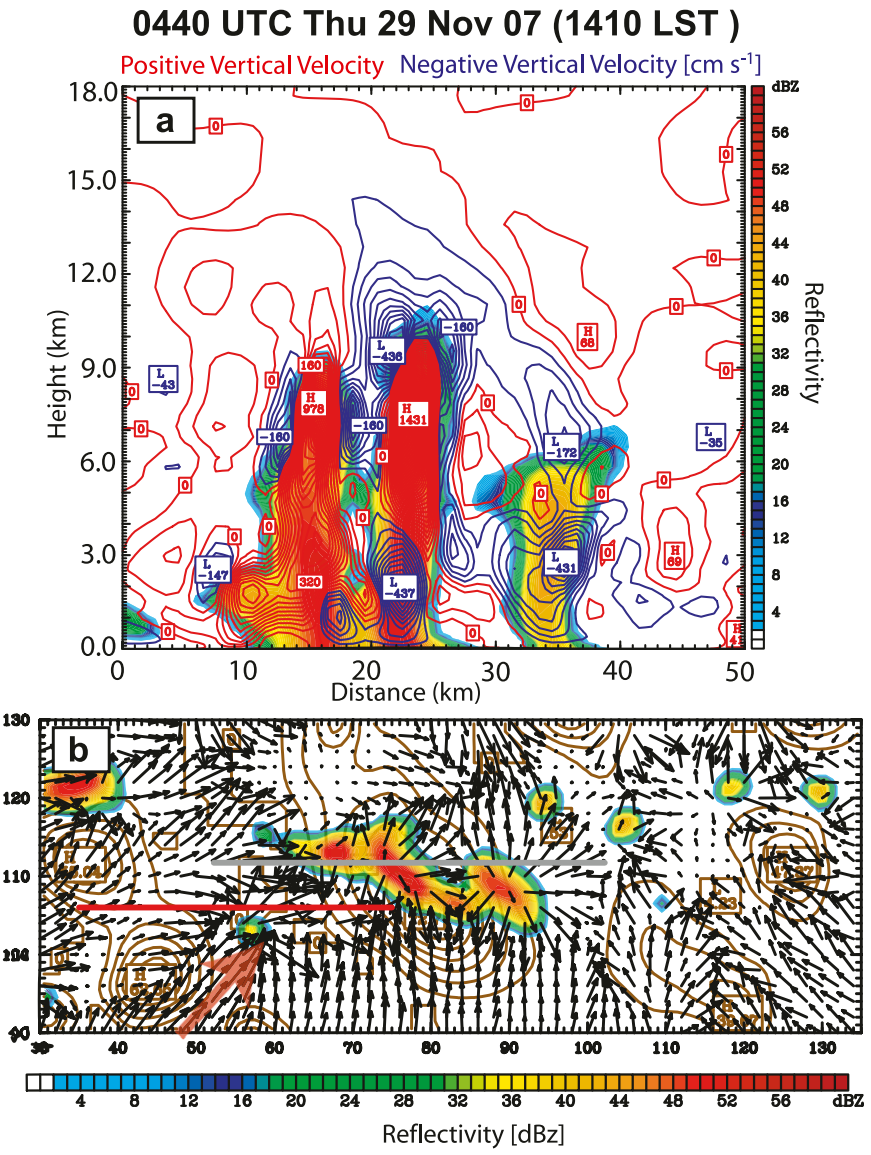

FIG. 11. Sections of the Hector triggering; the vertical one is taken along the solid gray line. (a) Positive and negative vertical velocity (cm s^{-1}; red and blue contours, respectively) and simulated radar reflectivity (dBZ; filled colors). (b) The simulated radar reflectivity (dBZ; filled colors) and the circulation vectors (arrows).

mechanisms: topography and previous precipitating convective cells. The first one acts by channeling the sea breeze in the valley producing gust winds. Hence, a convergence line is produced by the downdraft of the previous convective cells and the channeled sea breeze. These imply a Hector type B—in contrast with what was inferred using radar observations only, as in section 3.

c. *From the vigorous to the old phase*

A maximum simulated reflectivity of 60 dBZ is reached at 1510 LST (Figs. 13 and 14d). At this time, Hector is at the maximum development with the top reaching 18 km (Fig. 13a). The cell width produced by MM5 is comparable with the one detected by TMI at the maximum development. In the next hour, the precipitating cell moves westward (Fig. 14e) and completely disappears at 1630 LST (Fig. 14f). The Berrimah radar at 1715 LST (Fig. 5d) recorded cells along the central axis of Tiwi Islands and in the next 20 min (at 1735 LST; not shown) recorded the cells moving farther southwestward; by 1745 LST, the cells move northwestward, initiating the decay phase of Hector.

TRMM overpasses the Tiwi Islands at the maximum development of the event, allowing for a comparison

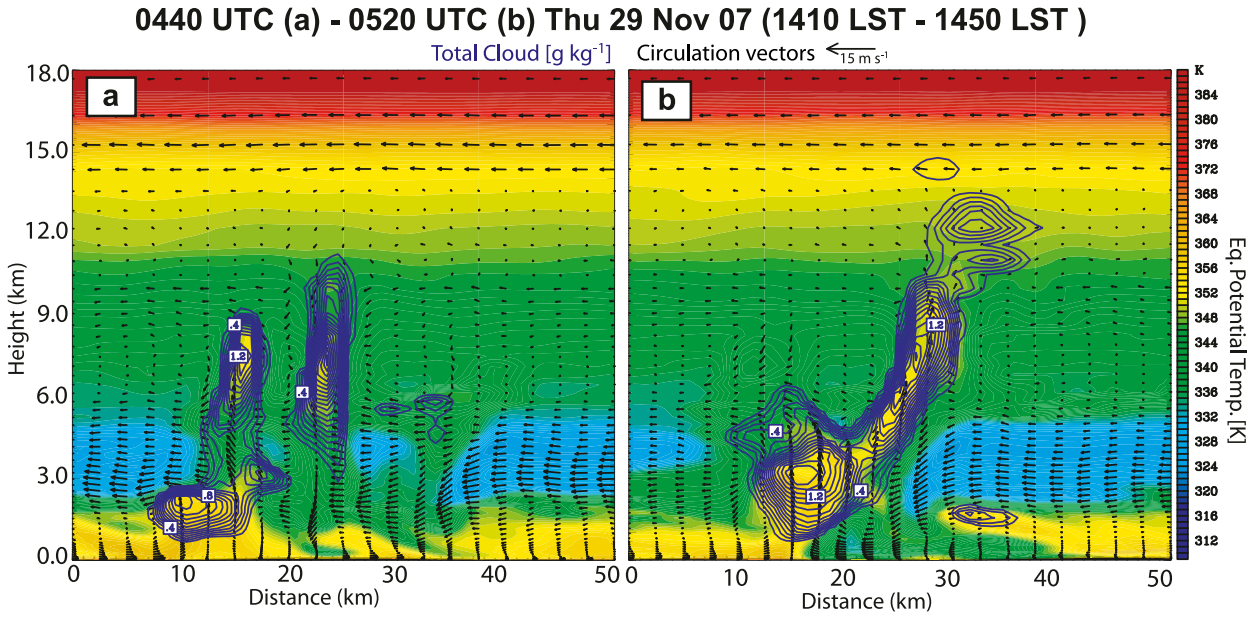

FIG. 12. Vertical sections of the simulated Hector embryo; the section is taken along the solid red line. Equivalent potential temperature (K; filled colors), total cloud-mixing ratio (g kg^{-1}; blue contours), and circulation vectors (arrows) at (a) 1410 and (b) 1450 LST.

between MM5 and TMI data in terms of hydrometeor vertical profiles. To ease the comparison between the MM5 microphysics and the TMI data within the convective cell, only the volume encapsulating Hector is selected. Because of the MM5 time displacement, the volume encapsulating Hector is chosen based on the stage of the cell and not at the time of TRMM overpass. This turns in a temporal and spatial bias removal from the high-resolution simulation. Hence, MM5 hydrometeors are taken at 1510 LST, whereas TMI data are at 1718 LST.

Two hydrometeors retrieved from TMI observation are extracted from the selected volume: precipitation ice water and precipitation liquid water. The mean vertical profiles for both precipitating hydrometeors are computed within the volume. The comparison between MM5 and TMI mean vertical profiles of mean precipitating ice and water (Figs. 15a,b; MM5 gray and TMI black lines) clearly shows a good agreement between the model and observation. Indeed, both the position of the maxima (slightly overestimated) and the vertical distribution are correctly reproduced by MM5 (Figs. 15a,b). The standard deviation is used in Figs. 15a and 15b to represent the spatial uncertainty of the TMI mean. The TRMM literature does not explicitly report a quantitative error for TMI-retrieved hydrometeor contents. The bars (Figs. 15a,b) indicate the variation or ''dispersion'' from the average. Note that averaging a horizontal section necessarily accounts for variation from high values (in the central area of the cell) to relatively low ones (along the edge); that is why very large deviations are found. Although the dispersion is large, the mean profiles obtained from the MM5 control simulation are in good agreement with the ones by TMI for both the hydrometeors (Figs. 15a,b).

A remarkable characteristic of this event is the considerable hydrometeor contents (Figs. 15a,b); the large amount of precipitation ice is most likely produced by the strong updraft during the vigorous convection, allowing for particles to grow by riming, as assessed by Houze's conceptual model (Houze 1997). During the old stage (i.e., stratiform following Houze's definition), the still-active upper-level updraft allows for the smaller particles to grow and for the bigger ones to fall as the large values of mean precipitation water suggest (Fig. 15b; MM5 gray and TMI black lines). As the updraft weakens, riming becomes less effective, allowing for particles to grow by vapor diffusion. The increased width of the top of the cell (Fig. 13a) would suggest lateral spreading going on for the light particles, agreeing well with Houze's conceptual model.

A bimodal structure of the vertical velocity is clearly shown in the MM5 time series of the vertical velocity following Hector (Fig. 16a): two maxima at different levels are found in good agreement with Houze's studies on the vertical structure of mesoscale convective system (MSC) in the tropical regions (Houze 1982, 1989, 1997). The different levels and timing of the two maxima would suggest two different precipitating phases, as hypothesized by Houze's conceptual model (Houze 1997): the convective phase and the stratiform phase. The low-level

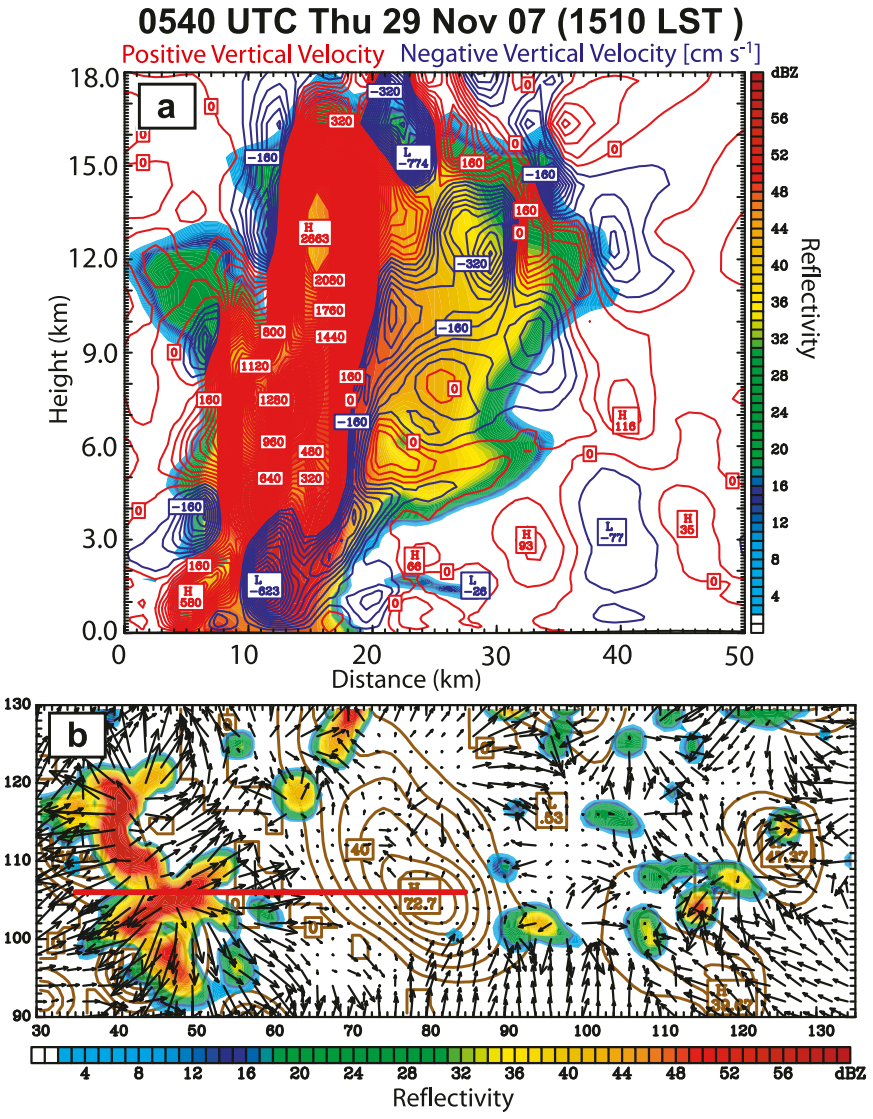

FIG. 13. Sections of the simulated Hector mature stage; the section is taken along the solid red line at 1510 LST. (a) Simulated vertical radar reflectivity (dB*Z*; filled color) and vertical velocity (red lines positive and blue lines negative). (b) Horizontal radar reflectivity (dB*Z*; filled color), topography (brown), and horizontal wind at the surface (arrows).

maximum of the vertical velocity, occurring before the one at higher level, is related to the vigorous convection, whereas the upper-level one is related to old convection (Houze 1997)—that is, the stratiform phase. The first phase has the maximum at approximately 8 km, whereas the second one is related to the stratiform part of the storm at 12–14 km (Fig. 16a); both well agree with what is observed in the tropical region (Houze 1989). In addition, the comparison of the mean vertical velocity between the observations for tropical island cases (Houze 1989) and the MM5 simulation (not shown) shows fair agreement between the two maxima: 1.6 m s^{-1} for the first and 0.6 m s^{-1} for the second. This small discrepancy may be caused by two different factors: 1) the MM5 value also contains the stratiform part of the cell, which is much slower than the convective one, and 2) the more complex orography of the island of Pohnpei, reaching approximately 600–800 m, than the orography of the Tiwi Islands (Houze 1989), which enhances the updraft. Support of this last hypothesis comes from the MM5 simulation without the southern orography (NOTOPO), showing values of vertical velocity that are half of the control simulation (Fig. 15c).

Moreover, the heating rate for both the liquid and ice processes associated to the Hector mature stage agree well (Fig. 16b, at 1450 LST) with Houze's conceptual

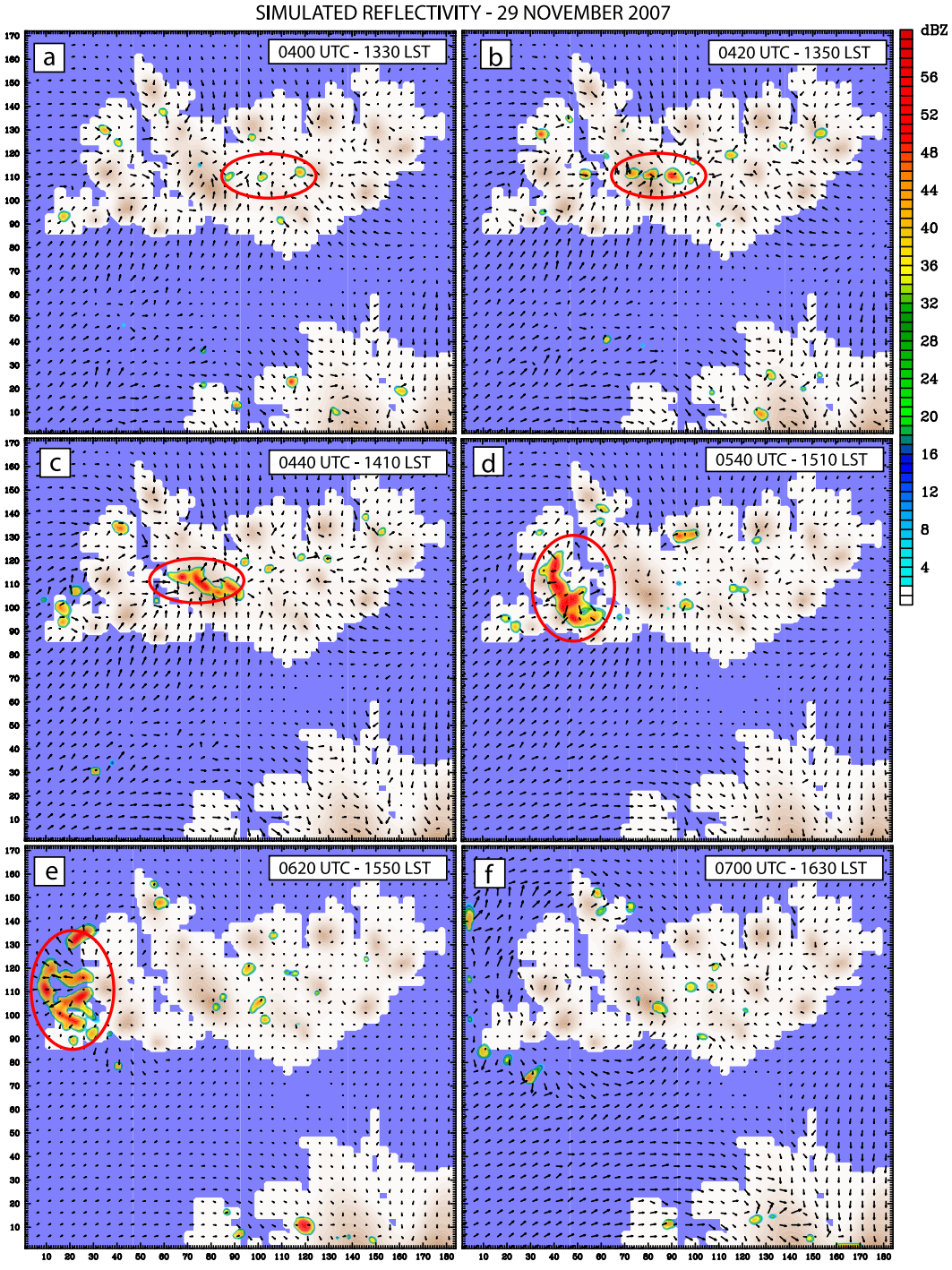

FIG. 14. MM5 simulated reflectivity from 1330 LST (0400 UTC) to 1630 LST (0700 UTC) 29 Nov 2007. Red circles indicate the convective cell locations.

model (Houze 1997). This roughly shows positive values for the whole depth of the atmosphere during the vigorous convection stage (until 1450 LST) and negative values at lower levels and positive at upper levels during the old stage—that is, from 1450 LST (Fig. 16b).

In addition, further details on the Hector structure can be found in Fig. 16c, reporting in filled colors the vertical profile of the equivalent potential temperature and in black contours the vertical velocity using an Eulerian approach; the time evolution of the variables has been

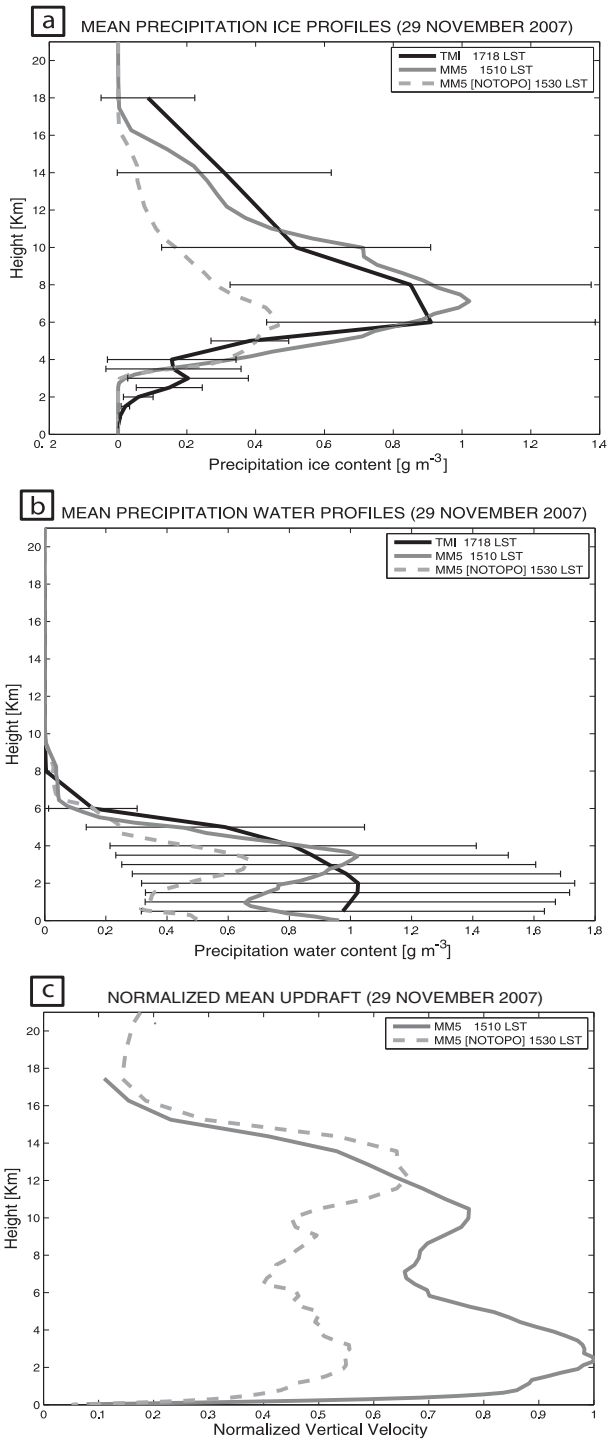

FIG. 15. The mean vertical profiles for 29 Nov 2007 event: (a) precipitation ice content, (b) precipitation water content, and (c) simulated vertical velocity. The black lines are relative to TMI at 1718 LST plus the standard deviation. The solid dark gray and the dashed light gray lines are for MM5 control simulation at 1510 LST and for MM5 NOTOPO at 1530 LST, respectively. The MM5 normalized mean updrafts are computed by averaging in both space and time and normalized to the maximum of the vertical velocity of MM5 control simulation.

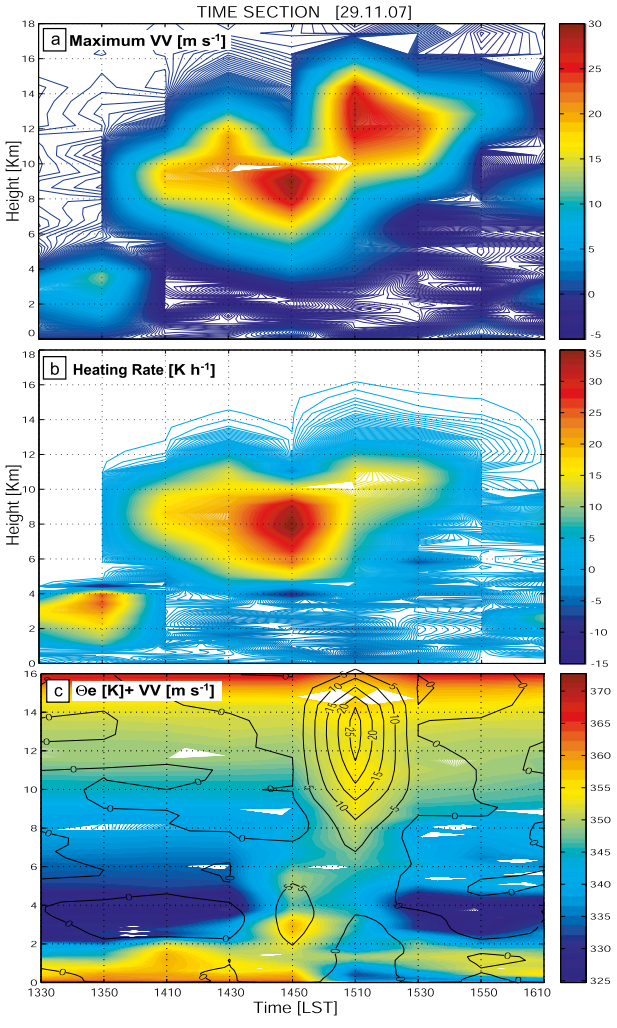

FIG. 16. Time section from 1330 to 1610 LST of (a) the simulated maximum vertical velocity ($m\,s^{-1}$) in the Lagrangian approach, (b) the heating rate ($K\,h^{-1}$) in the Lagrangian approach, and (c) the equivalent potential temperature (K; filled colors) with vertical velocity ($m\,s^{-1}$; black contours) in the Eulerian approach.

evaluated at the location of the maximum development. Instead, Figs. 16a and 16b used a Lagrangian approach—that is, following the Hector cell. Figure 16c clearly shows the onset of the sea breeze in the lower levels with the increase of the moist static energy from 1330 LST and the triggering stage (1450 LST) with the upward motion breaking the cold and dry layer. From 1450 LST, the equivalent potential energy lifts up to 6 km, sustained by an updraft of approximately $5\,m\,s^{-1}$, reaching the maximum vertical velocity at higher levels at 1510 LST. After this vigorous phase, the moist static energy decreases at all levels and the dry and cold layer between 2 and 6 km is renovated. At the lower layers, the wet advection is still occurring from the southern coast.

6. Conclusions

A study of the triggering mechanisms and microphysical structure of a Hector event was presented. The case was analyzed using MM5 simulations, ground-based radar reflectivity, and TRMM satellite data to the aim of understanding the vertical structure and the dynamical evolution of the storm. The analysis of the horizontal and vertical structure at high temporal and spatial resolution produced by MM5 allowed us to understand the mechanisms for triggering Hector and to support Houze's conceptual model for tropical convection (Houze 1997). The sketch in Fig. 17 illustrates the life cycle of the storm, summarizing the main processes contributing to the Hector development. Three different stages characterize the storm:

- The pre-Hector phase, when thermal convection is triggered by the slow air motion of the northern sea breeze over the warm surface, ending as the downdraft associated with the precipitation starts interacting with the well-organized upward and downward motion of the convective cells (Fig. 17).
- The triggering phase, when early convection develops over the southern side of the Tiwi Islands triggered by southern sea breeze front, bringing warm and humid air inland and lifting by the small hills (Fig. 17). As the two sea-breeze fronts move farther inland, scattered convection develops. Finally, over the southern side of the islands a channeling effect, due to small hills, is strengthened by the sea-breeze front, causing a convergence line that interacts with the downdraft of a convective cell, and triggering Hector. The NOTOPO simulation (i.e., disregarding the southern topography) supports this hypothesis simulating a weaker maximum convective cell and producing much less total condensate than the one produced by the control simulation.
- The final phase, when the vigorous convection and the following old stage are characterized by hydrometers at different levels associated with a different vertical velocity structure. Both the vertical velocity and the heating rate time series support Houze's conceptual model for the tropical convection by producing a bimodal structure and a varying vertical distribution depending on the stage of the convection. Moreover, the vertical distribution of both precipitation ice and precipitation water produced by MM5 agrees with that retrieved by TMI.
- The model and observation analysis allows us to assess the Hector type B for this event, whereas the observation would suggest a type A.

The overall analysis suggests that the most important factors for the 29 November 2007 event, which is characterized by a large amount of total condensate, are the low surface wind velocity with a favorable direction and the wet advection. The first factor allows for lower-level air to warm up, increasing the buoyancy as the large value of CAPE suggests.

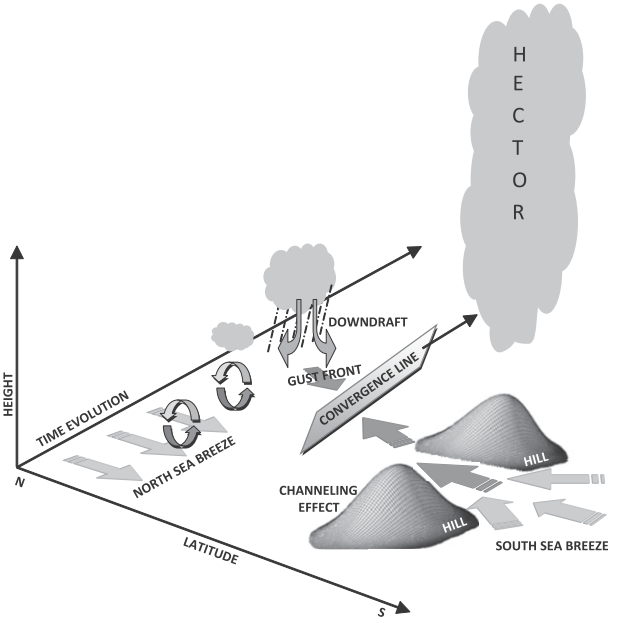

FIG. 17. Sketch illustrating the life cycle of the storm.

There are still several uncertainties in the Hector vertical structure, as well as, in general, in tropical thunderstorms, especially concerning the different mechanisms of hydrometeor production at different levels in the vigorous and old stages. Specific numerical experiments will be performed in future work using a high-resolution model and a cloud-resolving model to verify if the main mechanism for producing ice during the vigorous convective phase is the riming process becoming less effective as the updraft weakens, allowing for particles to grow by water vapor diffusion (Houze 1997).

Acknowledgments. R. Carbone is acknowledged for his helpful discussion on the form of one Hector event. Michael Whimpey and Peter May are acknowledged for the satellite imagery. NCAR is acknowledged for the MM5. NASA GSFC is acknowledged for the TMI data. ECMWF is acknowledged for data analysis. Todd Smith and Bureau of Meteorology of Australia are acknowledged for Berrimah radar imagery. Ernani De Lima Nascimento is acknowledged for the revision of the text.

REFERENCES

Ballard, S., B. Golding, and R. Smith, 1991: Mesoscale model experimental forecasts of the haar of northeast Scotland. *Mon. Wea. Rev.,* **119,** 2107–2123.

Carbone, R., J. Wilson, T. Keenan, and J. Hacker, 2000: Tropical island convection in the absence of significant topography. Part I: Life cycle of diurnally forced convection. *Mon. Wea. Rev.,* **128,** 3459–3480.

Crook, N., 2001: Understanding hector: The dynamics of island thunderstorm. *Mon. Wea. Rev.,* **129,** 1550–1563.

Dudhia, J., 1993: A nonhydrostatic version of the Penn State–NCAR mesoscale model: Validation tests and simulations of an Atlantic cyclone and cold front. *Mon. Wea. Rev.,* **121,** 1493–1513.

——, G. Dave, K. Manning, W. Wang, and C. Bruyere, 2005: PSU/NCAR Mesoscale Modeling System tutorial class notes and users' guide: MM5 Modeling System version 3. National Center for Atmospheric Research Mesoscale and Microscale Meteorology Division Tech. Note, 402 pp.

Ferretti, R., and S. Gentile, 2009: A study of the triggering mechanisms for deep convection in the tropics using a mesoscale model: Hector events during SCOUT-O_3 and TWP-ICE campaigns. *Atmos. Res.,* **93,** 247–269.

Goddard Space Flight Center Distributed Active Archive Center, 2007: Volume 4: File specifications for TRMM products—Level 2 and Level 3. Tropical Rainfall Measuring Mission science data and information system—Interface control specification between the Tropical Rainfall Measuring Mission Science Data and Information System (TSDIS) and the TSDIS Science User (TSU), NASA Goddard Space Center Tech. Note, 82 pp.

Golding, B., 1993: A numerical investigation of tropical island thunderstorms. *Mon. Wea. Rev.,* **121,** 1417–1433.

Grell, G., J. Dudhia, and D. Stauffer, 1994: A description of the Fifth-Generation Penn State/NCAR Mesoscale Model (MM5). NCAR Tech. Note NCAR/TN-398+STR, 122 pp.

Houze, R., 1982: Cloud clusters and large-scale vertical motions in the tropics. *J. Meteor. Soc. Japan,* **60,** 396–410.

——, 1989: Observed structure of mesoscale convective systems and implications for large-scale heating. *Quart. J. Roy. Meteor. Soc.,* **115,** 425–461.

——, 1997: Stratiform precipitation in regions of convection: A meteorological paradox? *Bull. Amer. Meteor. Soc.,* **78,** 2179–2196.

Kain, J., 2004: The Kain–Fritsch convective parameterization: An update. *J. Appl. Meteor.,* **43,** 170–181.

——, and J. Fritsch, 1993: Convective parameterization for mesoscale models: The Kain-Fritsch scheme. *The Representation of Cumulus Convection in Numerical Models, Meteor. Monogr.,* No. 46, Amer. Meteor. Soc., 165–170.

Keenan, T., and R. Carbone, 1992: A preliminary morphology of precipitation system in tropical northern Australia. *Quart. J. Roy. Meteor. Soc.,* **118,** 283–326.

Kummerow, C., and Coauthors, 2000: The status of the Tropical Rainfall Measuring Mission (TRMM) after two years in orbit. *J. Appl. Meteor.,* **39,** 3170–3187.

Reisner, J., R. Rasmussen, and R. Bruintjes, 1998: Explicit forecasting of supercooled liquid water in winter storms using the MM5 mesoscale model. *Quart. J. Roy. Meteor. Soc.,* **124,** 1071–1107.

Saito, K., T. Keenan, G. Holland, and K. Puri, 2001: Numerical simulation of the diurnal evolution of tropical island convection over the Maritime Continent. *Mon. Wea. Rev.,* **129,** 378–400.

Shafran, P., N. Seaman, and G. Gayno, 2000: Evaluation of numerical predictions of boundary layer structure during the Lake Michigan ozone study. *J. Appl. Meteor.,* **39,** 412–426.

Stoelinga, M., 2009: A users' guide to RIP version 4.5: A program for visualizing mesoscale model output. UCAR Mesoscale and Microscale Meteorology Rep., 82 pp. [Available online at http://www.mmm.ucar.edu/wrf/users/docs/ripug.pdf.]

Stull, R., 1988: *An Introduction to Boundary Layer Meteorology.* Kluwer Academic Press, 666 pp.

Vulpiani, G., F. Marzano, V. Chandrasekar, and S. Lim, 2005: Constrained iterative technique with embedded neural-network for dual polarization radar correction of rain path attenuation. *IEEE Trans. Geosci. Remote Sens.,* **43,** 2305–2314.

Zipser, E., D. Cecil, C. Liu, S. Nesbitt, and D. Yorty, 2006: Where are the most intense thunderstorms on Earth? *Bull. Amer. Meteor. Soc.,* **87,** 1057–1071.